ACS APPLIED MATERIALS & INTERFACES

Research Article

Cite This: ACS Appl. Mater. Interfaces 2018, 10, 31080−31087

www.acsami.org

Ultrasensitive Photoelectrochemical Biosensing Platform for Detecting N-Terminal Pro-brain Natriuretic Peptide Based on SnO_2/SnS_2/mpg-C_3N_4 Amplified by PbS/SiO_2

Yifeng Zhang,[†] Rui Xu,[†] Qing Kang,[‡] Yong Zhang,[†] Qin Wei,*[,†] Yaoguang Wang,*[,†] and Huangxian Ju[†]

[†]Key Laboratory of Interfacial Reaction & Sensing Analysis in Universities of Shandong, School of Chemistry and Chemical Engineering, and [‡]Institute of Surface Analysis and Chemical Biology, University of Jinan, Jinan 250022, P. R. China

Supporting Information

ABSTRACT: A sandwich-type photoelectrochemical (PEC) immunosensor for detecting N-terminal pro-brain natriuretic peptide (NT-proBNP) was constructed on the basis of SnO_2/SnS_2/mpg-C_3N_4 nanocomposites and PbS/SiO_2, with the former as a photoactive matrix and the latter as an efficient quencher. SnO_2/SnS_2/mpg-C_3N_4 was synthesized via in situ growth of SnO_2 and SnS_2 on mesoporous graphene like C_3N_4 nanocomposites (mpg-C_3N_4). Specifically, SnO_2/SnS_2/mpg-C_3N_4 exhibited intense PEC signal responses, which are tens of times stronger than its each single component. Because of its superior performance, SnO_2/SnS_2/mpg-C_3N_4 was applied as a photoactive matrix and signal indicator for fabricating PEC immunosensor. Interestingly, the excellent PEC signals from SnO_2/SnS_2/mpg-C_3N_4 could be reduced severely with the addition of PbS/SiO_2. Hence, the secondary antibody bioconjugates (PbS/SiO_2-Ab_2) were prepared as an efficient quencher. The mechanism of the quench reaction was further discussed in detail. On the basis of the interaction between the matrix and the quencher, the NT-proBNP immunosensor was fabricated and a wide linear range of 0.1 pg·mL^{-1} to 50 ng·mL^{-1} was obtained with a low detection limit of 0.05 pg·mL^{-1}. Additionally, the PEC immunosensor manifested good stability, reproducibility, and selectivity, which could underlie robust platforms for detecting multitudinous biomarkers or other targets of interest.

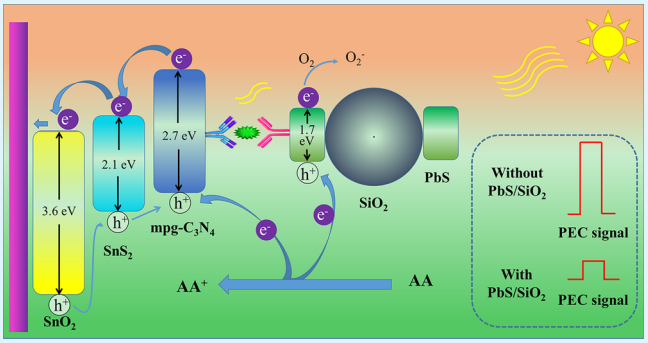

KEYWORDS: *photoelectrochemical immunosensor, sandwich-type, PbS/SiO_2, SnO_2/SnS_2/mpg-C_3N_4, NT-proBNP*

INTRODUCTION

N-terminal pro-brain natriuretic peptide (NT-proBNP), a biologically active natural hormone, is synthesized by cardiomyocytes, mainly expressing in the ventricle and brain tissue.[1,2] Because plenty of evidence has found that its level has increased among patients with cardiovascular and cerebrovascular diseases, NT-proBNP is acknowledged as a reliable biomarker of heart failure.[3,4] Therefore, the early detection of abnormal NT-proBNP content is significant for the timely diagnosis and treatment of the disease.[5] Currently, various sensing methods, such as enzyme-linked immunosorbent assay, fluorescence, electrochemiluminescence, and photoelectrochemical (PEC) assay, have been developed for biomarker detection.[5−9] Of these detection technologies, PEC assay takes on some unique advantages encompassing high sensitivity, low background signal, easy miniaturization, low cost, and simple operation, getting hold of widespread attention in accurate bioanalysis in recent years.[10]

For PEC immunosensors, photoelectric active species have a vital influence on the performance of the immunosensor.[11] To date, a variety of organic and inorganic semiconductor materials with high photo-to-current conversion efficiency have been applied to fabricate PEC detection platforms, especially TiO_2 and CdS.[12,13] However, TiO_2 has no photoresponse in the visible range in virtue of the broad band gap, whereas CdS is prone to photocorrosion and takes on unstable performance.[14] To solve these problems, many studies aim to enhance the photoelectric properties by doping, compounding, and sensitizing treatments.[15−17] However, the synthetic procedure of the material would be fussy and tedious. Hence, developing highly active photoelectrical materials with simple synthetical methods is still desirable for constructing highly sensitive PEC immunosensors.

SnO_2, as a stable conductive material, has been widely employed in lithium batteries, gas sensor, capacitor, and other fields, but it needs to be doped, sensitized, or coupled when it comes to its application in photocatalysis on account of its large band gap about 3.6 eV.[18−20] SnS_2, a nontoxic n-type

Received: July 7, 2018
Accepted: August 29, 2018
Published: August 29, 2018

DOI: 10.1021/acsami.8b11312
ACS Appl. Mater. Interfaces 2018, 10, 31080−31087

Scheme 1. (A) Schematic Illustration for the Construction of PEC Immunosensor; (B) Photocurrent-Generating (Left) and Photocurrent-Quenching (Right) Mechanisms

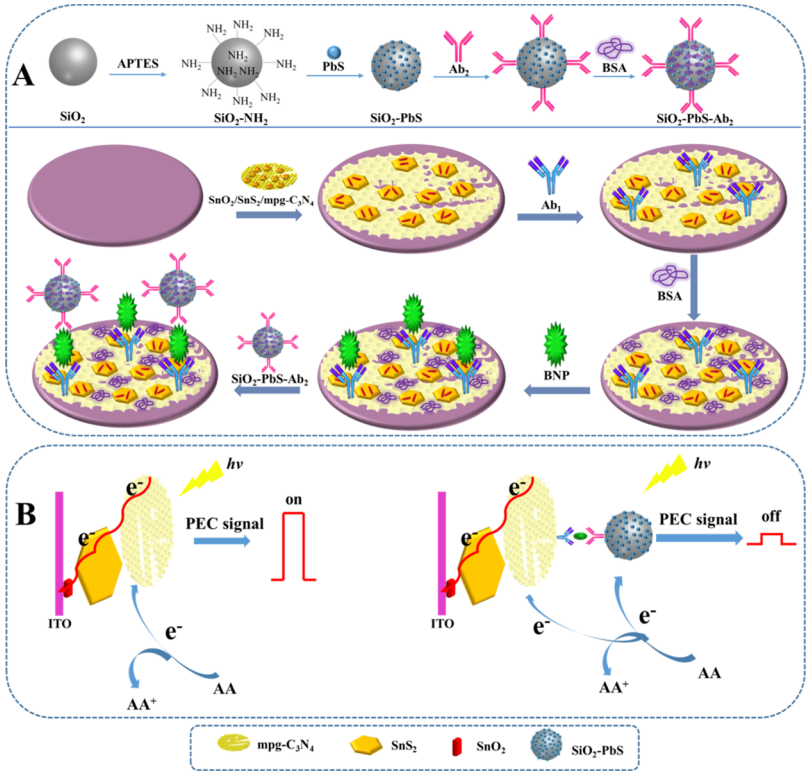

semiconductor, takes on a suitable forbidden bandwidth (~2.2 eV), coupled with good stability under nonalkaline conditions, making it shine in photocatalysis and photodegradation field.[21] It is reported that SnS_2 coupled with other semiconductors such as SnO_2 yields better photocatalytic effect than its single component, but its photoelectric conversion efficiency still needs to be further improved when applied to PEC sensing.[22] Mesoporous carbon nitride (mpg-C_3N_4) has an extensive use in photodegradation because of its appropriate band gap (~2.7 eV) and high specific surface area. Its porous structure augments the electron capture sites and slows the recombination of photogenerated electron−hole pairs, making it possible to overcome the adverse effects of a slight increase in band gap to improve the photoelectric conversion efficiency.[23] Moreover, its special structure provides numerous loading sites for other materials. In this work, we synthesized the novel eco-friendly SnO_2/SnS_2/mpg-C_3N_4 nanocomposites by in situ growth of SnO_2 and SnS_2 on carbon nitride in a one-pot process. Compared with Yang's work, we have greatly simplified the experimental steps.[24] The as-prepared SnO_2/SnS_2/mpg-C_3N_4 takes on high photoelectric conversion efficiency in the visible region because of the good energy level matching of the three components. It is also worth noting that we introduced carboxyl groups on the surface of mpg-C_3N_4 by carboxylation, which could facilitate the bonding with proteins.

As is well known, efficient quenchers play indispensable roles in constructing signal-off immunosensors with high sensitivity. Recently, a new p−n-type quenching model was proposed and demonstrated to be very effective since p-type semiconductors could compete to absorb lights and electron donors of signal indicators.[25] For instance, PbS quantum dots (PbS QDs) as efficient p-type quenchers were singled out to quench anodic photocurrent which was generated by n-type semiconductors in PEC immunosensors.[26] SiO_2 possesses characteristics encompassing controllable morphology, easy function, poor conductivity, and large steric hindrance; therefore, we chose it as a carrier to load more PbS QDs to form PbS/SiO_2 and achieve higher quenching efficiency.

As Scheme 1A illustrated, an original sandwich-type PEC immunosensor was fabricated on the basis of SnO_2/SnS_2/mpg-C_3N_4 coupled with efficient quencher-PbS/SiO_2 for ultrasensitive detection of NT-proBNP. The carboxyl groups attached on mpg-C_3N_4 can be directly linked to the antibody after EDC/NHS activation. After blocking nonspecific active sites with bovine serum albumin (BSA), the hatched antigen would combine with the antibody to form an immune complex which possesses huge steric-hindrance effect, causing a decrease in photocurrent. To further amplify the signal change, the electrodes were modified with PbS/SiO_2-Ab_2. In comparison to reducing photocurrent merely by stereo-hindrance effect of immune complexes, the addition of PbS/SiO_2 further lessened the production of photocurrent through competitive consumption of light and hole-trapping agent of PbS and high steric hindrance effect of SiO_2. Light with the wavelength of 450 nm was employed as the stimulus, whereas ascorbic acid (AA) served as a hole-trapping agent that greatly enhanced the photoelectric conversion efficiency. The as-established sandwich-type PEC detection platform exhibited good performance with excellent selectivity, reproducibility, and stability, which promised it to be a potent channel for detecting NT-proBNP.

EXPERIMENTAL SECTION

Synthesis of SnO_2/SnS_2/mpg-C_3N_4 Nanocomposites. Mpg-C_3N_4 was prepared by reference to the literature, and the details are

DOI: 10.1021/acsami.8b11312
ACS Appl. Mater. Interfaces 2018, 10, 31080−31087

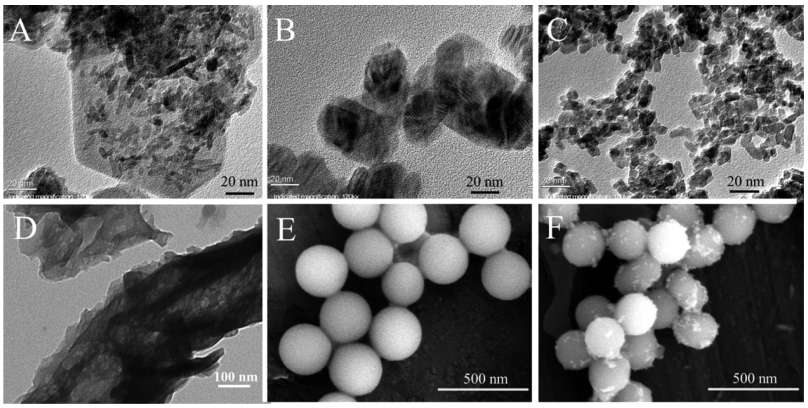

Figure 1. HRTEM images of (A) SnO_2/SnS_2/mpg-C_3N_4, (B) SnS_2, (C) SnO_2, and (D) mpg-C_3N_4. FESEM images of (E) SiO_2 and (F) PbS/SiO_2.

shown in Supporting Information.[27] SnO_2/SnS_2/mpg-C_3N_4 nanocomposites were prepared in a one-pot hydrothermal process. Specifically, mpg-C_3N_4 with different mass was added into 35 mL ultrapure water followed by ultrasound dispersion for 10 min. $SnCl_4 \cdot 5H_2O$ (5 mmol) was added to the aforementioned solution under violent agitation subsequently. After being stirred for 20 min, a certain amount of thio acetamide (TAA) was mixed into the above solution (the details about the doses of mpg-C_3N_4 and TAA are shown in Table S1 (Supporting Information) and the products synthesized by different amounts of feedstock were named composites a–j). The homogeneous solution which was electromagnetically stirred for 30 min was transferred into a teflon-sealed autoclave with 50 mL volume and heated to 190 °C for 6 h to obtain the target product. The autoclave was allowed to cool to room temperature naturally followed by washing the resulting product with ultrapure water and ethanol thoroughly in turn. Finally, the precipitate was dried in an vacuum oven at 60 °C overnight.

Preparation of PbS/SiO_2-Ab_2 Bioconjugates. The synthesis of SiO_2–NH_2 and thermogravimetric analysis (TGA)-capped PbS was performed according to the method given in the literature with minor improvement.[28,29] The detailed synthetic steps of PbS/SiO_2 are as follows: first, 10 mg of SiO_2–NH_2 was dissolved in 30 mL of PbS QDs solution in which 0.76 g of EDC and 0.11 g of NHS were added in advance. After that, the solution was stirred for 2 h at room temperature to get dark gray PbS/SiO_2. Finally, the obtained PbS/SiO_2 was washed with ultrapure water three times and dried at 60 °C in vacuum oven for 12 h.

In terms of the synthesis of PbS/SiO_2-Ab_2, initially, 2 mL of 10 $\mu g \cdot mL^{-1}$ Ab_2, 10 μL of 5 $mg \cdot mL^{-1}$ EDC, and 10 μL of 1 $mg \cdot mL^{-1}$ NHS were mixed and oscillated for 30 min at 4 °C in constant temperature oscillation incubator. Second, 5 mg of PbS/SiO_2 was added into the above solution. BSA (100 μL, 1 w %) was injected into the solution after it was incubated for 12 h. After being oscillated for 30 min at room temperature, the reaction solution was washed with PBS three times. Finally, the precipitation was dispersed in 2 mL of PBS and placed in 4 °C refrigerator for later use.

PEC Immunosensor Construction. The working electrode of the immunosensor was built on the basis of indium tin oxide (ITO) glass (1 cm × 2.5 cm). Next, they were ultrasonically treated for 30 min in various solutions in such an order-ultrapure water, acetone, ultrapure water, ethanol, and ultrapure water, followed by immersing the ITO glass in 1 $mol \cdot L^{-1}$ NaOH solution overnight at room temperature. After being washed with ultrapure water, the ITO glass were dried in drying cabinet at 70 °C for 4 h for further use.

For the fabrication of working electrodes, initially, 6 μL the homogeneous SnO_2/SnS_2/mpg-C_3N_4 aqueous solution with a concentration of 3 mg/mL was dropped onto the conductive side of ITO slice. After natural air-drying, 4 μL of mixed aqueous solution containing EDC (0.01 $mol \cdot L^{-1}$) and NHS (0.02 $mol \cdot L^{-1}$) was adorned on the modified electrode. Until the modified electrode was naturally drying to water film condition, the redundant EDC and NHS were rinsed off with washing buffer. Subsequently, the above electrode was combined with 4 μL of Ab_1 solution with a concentration of 10 $\mu g \cdot mL^{-1}$ and was dried to wet film state at 4 °C, followed by washing away the Ab_1 physically adsorbed on the electrodes. To block nonspecific binding sites, 3 μL of BSA with a mass fraction of 1% was added onto the modified electrode in next step and was incubated to wet film state in 4 °C refrigerator, followed by swashing with washing buffer efficaciously. In the penultimate step, 4 μL NT-proBNP antigen solution with different concentrations were decorated onto different electrodes and hatched at 4 °C in thermostatic refrigerator followed by washing with the washing buffer carefully. PbS/SiO_2-Ab_2 bioconjugates solution (4 μL) was added onto the above modified electrodes. After being incubated at a constant temperature of 4 °C and being dried properly, the resulting electrodes were finally rinsed with the washing buffer carefully and employed as a sandwich PEC immunosensor for the later PEC tests.

Photocurrent Response Test. The experiment of photocurrent response test was carried out in PBS (pH = 7.4) containing AA (0.2 $mol \cdot L^{-1}$). The photocurrent was acquired with the help of a PEC workstation at 0 V bias voltage at room temperature and the excitation light that is 180 $W \cdot m^{-2}$ in intensity and 450 nm in wavelength.

RESULT AND DISCUSSION

Topography and Spectral Characterization of the Synthesized materials. High-resolution transmission electron microscopy (HRTEM) images and field emission scanning electron microscopy (FESEM) of the synthesized materials are shown in Figure 1. Figure 1B reveals that SnS_2 is flake-shaped and has a diameter of about 50 nm, whereas Figure 1C declares that SnO_2 is a rod having a size of about 10 nm. In combination with HRTEM image of SnO_2/SnS_2/mpg-C_3N_4 (Figure 1A), we can speculate that the sheet is SnS_2 and the rod is SnO_2. What is more, it is obvious that the SnS_2 flakes in the nanocomposites are larger in size and more dispersible when comparing Figure 1A with B. The HRTEM image of mpg-C_3N_4 (Figure 1D) reveals that mpg-C_3N_4 possesses a porous structure. Compared with thicker sheet-like SnS_2 and rod-shaped SnO_2, mpg-C_3N_4 is difficult to find in HRTEM image of SnO_2/SnS_2/mpg-C_3N_4 on account of its less content and thin-film mesoporous structure. It can be easily seen that the SiO_2 particles have uniformly spherical structure with the size about 200 nm according to Figure 1E. As shown in Figure 1F, PbS nanoparticles were successfully fixed on the surface of SiO_2. The measurement results show that the BET surface area of the as-synthesized mpg-C_3N_4 is about 157 $m^2 \cdot g^{-1}$ and the nitrogen adsorption–desorption isotherm is shown in Figure S1 (Supporting Information) which exhibits the type-H3 hysteresis loop characteristic of mesoporous materials (pore

DOI: 10.1021/acsami.8b11312
ACS Appl. Mater. Interfaces 2018, 10, 31080–31087

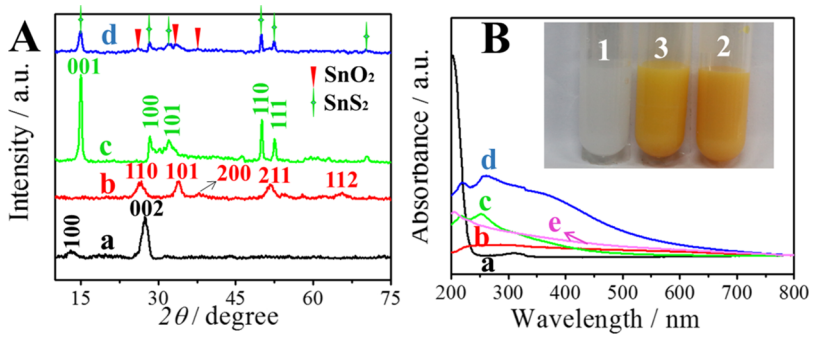

Figure 2. (A) XRD patterns of (a) mpg-C_3N_4, (b) SnO_2, (c) SnS_2, and (d) SnO_2/SnS_2/mpg-C_3N_4. (B) UV−vis absorption spectra of (a) mpg-C_3N_4, (b) SnO_2, (c) SnS_2, (d) SnO_2/SnS_2/mpg-C_3N_4, and (e) PbS/SiO_2 and centrifuge tubes 1, 2, and 3 embedded in (B) are SnO_2, SnS_2, and SnO_2/SnS_2/mpg-C_3N_4 solutions, respectively.

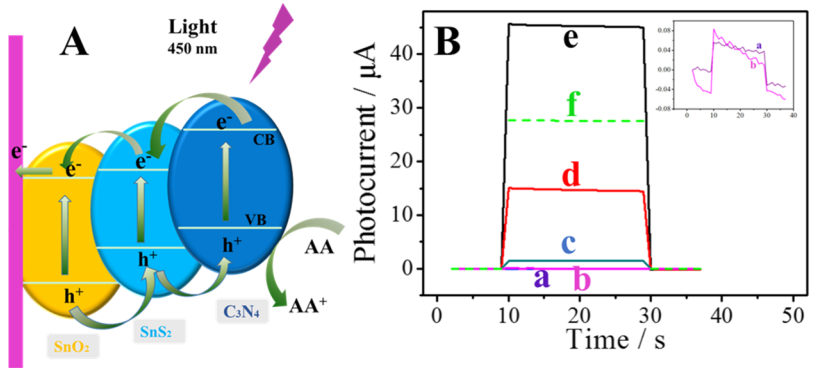

Figure 3. (A) Illustration of photo-induced electrons' transfer mechanism of the electrode decorated with SnO_2/SnS_2/mpg-C_3N_4. (B) Photocurrents of electrodes modified with (a) SnO_2, (b) mpg-C_3N_4, (c) SnS_2, (d) SnO_2/SnS_2, (e) SnO_2/SnS_2/mpg-C_3N_4, and (f) SnO_2/SnS_2/mpg-C_3N_4-PbS/SiO_2 (6 μL, 3 mg·mL^{-1}).

diameter, 2−8 nm). In addition, the XPS spectrum of SnO_2/SnS_2/mpg-C_3N_4 nanocomposites presented in Figure S2 and the binding energy of Sn $3d_{5/2}$, S $2p_{3/2}$, O 1s, C 1s and N 1s of SnO_2/SnS_2/mpg-C_3N_4 nanocomposites are in turn 486.5, 161.1, 530.9, 284.7, and 404.5 eV, which are consistent with the five elements included in SnO_2/SnS_2/mpg-C_3N_4.[30,31]

Figure 2A indicates the X-ray diffraction (XRD) patterns of the as-synthesized materials. As we can see, the pure mpg-C_3N_4 (curve a) presents a strong peak at 27.41°, which is characteristic of the stacking peak of pi-conjugated layers and is assigned to the (002) lattice plane of graphitic materials.[32] The weak peak at 13.1° indexed (100) lattice plane of CN. Those five conspicuously characteristic peaks (curve b) appearing at 26.6°, 33.9°, 37.9°, 51.8°, and 65.9° corresponds to five lattice planes-(100), (101), (200), (211), and (301) of tetragonal phase SnO_2 (JCPDS no. 41-1445). Curve c suggests that it is a hexagonal phase SnS_2 (JCPDS no. 23-0677) which owns characteristic peaks at 15°, 28.2°, 32.1°, 49.9°, and 52.5° corresponding lattice planes (001), (100), (101), (110), and (111).[30] The diffraction pattern of the nanocomposites is demonstrated by curve (d). In addition, we can easily reason out that the SnO_2/SnS_2/mpg-C_3N_4 nanocomposites were synthesized successfully. It is worth noting that the diffraction peaks of mpg-C_3N_4 are not shown in curve d because of its very low content. As manifested in Figure 2B, compared with those three kinds of single-phase materials, the absorption edge of the SnO_2/SnS_2/mpg-C_3N_4 nanocomposites is located on the far right and a great absorption in the 300−500 nm range. PbS/SiO_2 solution (curve e) exhibits absorption of light at the wavelength of the excitation light. The number 1, 2, and 3 tubes inserted in Figure 2B are the solution of SnO_2, SnS_2, and SnO_2/SnS_2/mpg-C_3N_4, respectively, with a concentration of 4 mg·mL^{-1}. It is easy to find that the as-synthesized SnO_2/SnS_2/mpg-C_3N_4 nanocomposites possess a brighter yellow color than that of SnS_2.

Mechanism Exploration. Sn^{4+} would be released when the $SnCl_4·5H_2O$ was added in the ultrapure water, while CH_3CSNH_2 would be hydrolyzed to produce H_2S. Whereafter, Sn^{4+} would react with H_2S and H_2O at the same time to generate SnS_2 and $Sn(OH)_4$ severally. However, the $Sn(OH)_4$ would immediately decompose into SnO_2 and H_2O. After the depletion of Sn^{4+}, excess H_2S could further react with SnO_2 to form SnS_2. As a result, the proportion of SnS_2 and SnO_2 in the product can be controlled by the dosage of CH_3CSNH_2 added.[30] The addition of a small amount of mpg-C_3N_4 was likely to serve as a platform for crystal growth which allowed the crystal to grow better.

As shown in Figure 3A, those three single-phase substances bear different valence band (VB) and conduction band (CB) energy levels, but they exhibit a ladder-like arrangement. According to energy band theory, photo-induced electrons would migrate along the path of the conduction band of mpg-C_3N_4 → SnS_2 → SnO_2 when the nanocomposites is exposed to light of 450 nm wavelength, reducing the recombination rate of photo-induced electron−hole pairs compared to single-phase material.[33,34] At the same time, AA contained in electrolyte solution would supply electrons to consume the photo-induced holes left in the VB of the nanocomposites, which further reduces the recombination rate of photogenerated electron−hole pairs, achieving a larger photocurrent.[35] Benefiting from

DOI: 10.1021/acsami.8b11312
ACS Appl. Mater. Interfaces 2018, 10, 31080−31087

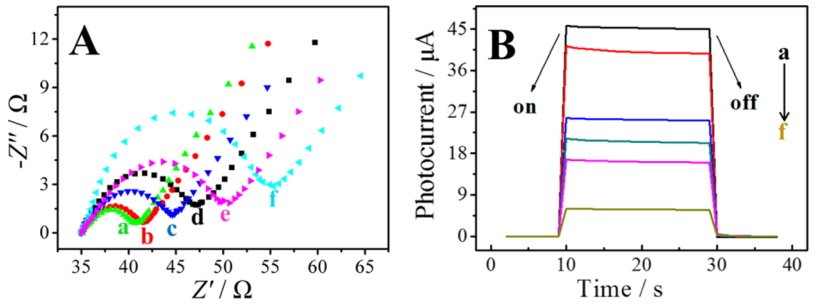

Figure 4. (A) Nyquist plots of EIS and (B) photocurrent responses in the different stages of the electrode modification: (a) SnO_2/SnS_2/mpg-C_3N_4, (b) SnO_2/SnS_2/mpg-C_3N_4/(EDC/NHS), (c) SnO_2/SnS_2/mpg-C_3N_4/(EDC/NHS)/Ab_1, (d) SnO_2/SnS_2/mpg-C_3N_4/(EDC/NHS)/Ab_1/BSA, (e) SnO_2/SnS_2/mpg-C_3N_4/(EDC/NHS)/Ab_1/BSA/NT-proBNP, and (f) SnO_2/SnS_2/mpg-C_3N_4/(EDC/NHS)/Ab_1/BSA/NT-proBNP/(PbS/SiO_2-Ab_2).

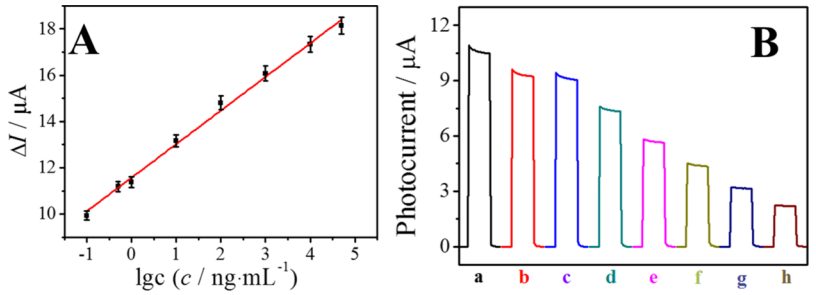

Figure 5. (A) Curves of photocurrent-logarithm of antigen concentration. $\Delta I = I_0 - I$, I_0 represents the photocurrent of the electrode decorated without bioconjugates and I is the photoresponse modified with bioconjugates. Error bars = SD (n = 3). (B) Photocurrent of the as-fabricated immunosensor with various concentration of NT-proBNP, (a to h) 0.1, 0.5, 1, 10, 100, 1000, 10 000, and 50 000 pg·mL^{-1}.

the above factors, it can be clearly seen from Figure 3B that SnO_2/SnS_2/mpg-C_3N_4 possesses the biggest photocurrent which is dozens of times the photoelectric conversion efficiency of single-phase materials. Nevertheless, a considerable decrease in photoresponse was obtained when the PbS/SiO_2 was furnished on the electrodes, which is because (6i) the p-type semiconductor could consume the light energy and electron donor belonging to SnO_2/SnS_2/mpg-C_3N_4; (ii) the poor electro-conductivity and large steric hindrance of SiO_2 obstructs the transfer of photo-induced electrons; and (iii) the introduction of SiO_2 increases the load of PbS which further enhances the quenching effect of PbS.

Characterization of the Immunosensors. To test the state of each modification process, electrochemical impedance spectroscopy (EIS) testing and time−photocurrent testing for each step of the immunosensor construction were performed and the results are shown in Figure 4A. EIS testing was carried out in electrolyte solution containing 5 mmol·L^{-1} $[Fe(CN)_6]^{3-/4-}$ and 0.1 mol·L^{-1} KCl with AC amplitude 5 mV and frequency 10^{-1} to 10^5 Hz without light. The bias voltage remained the default 0 V. Generally speaking, the EIS plots contain semicircle portion at higher frequencies and linear portion at lower frequencies, which represent electron-transfer-limited process and diffusion process. respectively.[36] As shown in Figure 4A, the impedance value of working electrodes gets bigger and bigger with the materials modified layer-by-layer. The electrode modified with SnO_2/SnS_2/mpg-C_3N_4 has the smallest diameter (curve a) and the electrode modified completely (the electrodes modified with SnO_2/SnS_2/mpg-C_3N_4/(EDC/NHS)/Ab_1/BSA/NT-proBNP/PbS/SiO_2-Ab_2) possesses the largest diameter (curve f) which means that the former has good conductivity and the latter takes on poor conductivity because of the nonconductive effect of the proteins. The spectra suggest that every step of the immunosensor construction is successful. Meanwhile, Figure 4B manifests the time−photocurrent test results of the working electrodes in different stages of modification. It is obvious that the electrode modified with SnO_2/SnS_2/mpg-C_3N_4 has the largest photocurrent owing to significantly enhanced photocurrent response (curve a), which is attributed to the high photoelectric conversion efficiency of SnO_2/SnS_2/mpg-C_3N_4. The photocurrent response is slightly reduced (curve b) after the modification of EDC/NHS which suggests that EDC/NHS is only used to activate the carboxyl groups on the surface of the composites and has little obstruction on the diffusion of AA. Ab_1 is excessive and causes a large decay in photocurrent (curve c). With the modification of BSA and NT-proBNP, photocurrent is further reduced. Benefiting from the insulation of anti-Ab_2 and the competitive absorbance of PbS/SiO_2, the photocurrent gets a big decrease after the modification of the bioconjugates and the reduced degree is larger relative to dropwise adding the antigen which indicates that the marker plays a magnifying role.

Optimization of Material and Immunosensor Performance. Within this research, the effects of different proportions of components belonging to SnO_2/SnS_2/mpg-C_3N_4 nanocomposites on photoresponse were investigated, and the results are shown in Table S1. From the table, we can see that the composite-i owned the largest photoresponse, and it was chosen as the optimal material for subsequent experiments such as characterization and immunosensor construction.

Becasue the photo-induced holes need to be consumed by the AA, the impact of AA content on the photocurrent is significant. Therefore, AA with different concentrations were acted as the electrolyte for the time−photocurrent test of the

DOI: 10.1021/acsami.8b11312
ACS Appl. Mater. Interfaces 2018, 10, 31080−31087

complete modified electrodes ($c_{NT\text{-}proBNP}$ = 100 pg·mL^{-1}). As we can see in Figure S3A, with the increase of AA concentration, photocurrent increased gradually, whereas the rate of increase decreased little by little. Taking into account economic factors and photocurrent stability, 0.2 mol·L^{-1} was selected as the best concentration. On the other hand, the antigenic activity and reducing power of AA are closely related to pH. PBS with different pH levels were used for testing, and pH 7.4 was proved to be the most suitable pH value.

PEC Detection for NT-proBNP. The difference in the amount of modified antigen results in a different effect on the electronic impediment. In this strategy, the more the antigen is modified, the more the photocurrent decreases. A series of electrodes modified by NT-proBNP solution with different concentrations were tested for photocurrent responses under optimal conditions, and the results are presented in Figure 5B. After data processing, it is found that the photocurrent value is linear with the logarithm of the concentration of NT-proBNP ranging from 0.1 pg·mL^{-1} to 50 ng·mL^{-1}. As shown in Figure 5A, the formula of this linear relationship is $\Delta I = 1.453 \lg c + 11.56$. What is more, the detection limit is calculated to be 0.05 pg·mL^{-1}. In a word, the proposed PEC immunosensor took on a wider detection range and a lower detection limit compared with most of the detection methods which can fully meet the daily testing needs (Table S2). The successful implementation of this strategy is of great significance for the rapid and sensitive detection of NT-proBNP.

Reproducibility, Selectivity, and Stability of the Immunosensor. Reproducibility reflects the reliability of the immunosensor, therefore, five identical electrodes modified with 100 pg·mL^{-1} NT-proBNP were used for repetitive testing under the same conditions and the calculated relative standard deviation (RSD) is 2.1% indicating that the fabricated immunosensor possessed good reproducibility.

A qualified immunosensor must bear good specificity to avoid false positives, thus reducing the misdiagnosis rate. Three representative antigens (PSA, CEA, and AFP) in human serum were tested for immunosensor selectivity by using interfering substances whose concentrations are as one-hundred times as that of NT-proBNP, which is 100 pg·mL^{-1}. It can be seen from Figure S4A that the interferents caused small changes in photocurrent within the error range (RSD = 2.6%), meaning a favorable selectivity of the fabricated PEC immunosensor for NT-proBNP detection.

Stability is a hard indicator of the immunosensor which manifests the stability of the immunosensor data. Thus, the stability of the immunosensor was evaluated in this work. The photoelectrical response test for a few on/off irradiation cycles with an interval of 20 s was recorded and the results are presented graphically in Figure S4B. As Figure S4B illustrates, it is obvious that there was no significant fluctuation in the photoresponse and the calculated RSD of the photocurrent value is 1.2% (n = 10), indicating satisfactory performance.

Actual Sample Test. The practicability and accuracy of the constructed PEC immunosensor were verified by testing the NT-proBNP concentration in human serum which was acquired from hospital with standard addition method. Standard NT-proBNP solutions with different concentrations and the serum samples were mixed for detection and the results are shown in Table S3. It can be seen from Table S3 that the average recoveries of the immunosensor were in the range of 95.8−100.9% with the RSD from 1.3 to 2.5%, indicating that the constructed PEC immunosensor could be safely applied in rapid clinical diagnosis in real samples.

CONCLUSION

In summary, SnO_2/SnS_2/mpg-C_3N_4 nanocomposites with high photoelectric conversion efficiency were first synthesized successfully with a one-pot method under mild conditions and employed as photoactive material to build a PEC detection platform for NT-proBNP analysis. Furthermore, the PbS/SiO_2 was synthesized and used as a label to amplify the photocurrent signal changes. Benefiting from the ladder-like energy level distribution of the three single-phase materials, photoexcited charges could be transferred quickly which largely reduces the recombination rate of photogenerated electron−hole pairs. Because the competitive absorption of exciting light and AA of PbS coupled with the high resistance of SiO_2, PbS/SiO_2 dramatically weakened the photocurrent response. The combination of the high photo-to-current conversion efficiency of SnO_2/SnS_2/mpg-C_3N_4 and the high photoelectric response inhibition of PbS/SiO_2 leads to a linear detection range of 0.1 pg·mL^{-1} to 50 ng·mL^{-1} with a detection limit of 0.05 pg·mL^{-1}. In addition, the simple, inexpensive, stable, and selective PEC detection platform has shown great potential in the field of biomarker detection and other related fields. Meanwhile, materials with better performance and simpler synthesis steps remain the goal of researchers to further improve the performance and convenience of sensors.

ASSOCIATED CONTENT

Supporting Information

The Supporting Information is available free of charge on the ACS Publications website at DOI: 10.1021/acsami.8b11312.

The Supporting Information is available free of charge and the contents are listed as follows: chemicals, apparatus, synthesis and functionalization of mpg-C_3N_4, preparation of SiO_2 and its functionalization, synthesis of TGA-capped PbS QDs, nitrogen adsorption−desorption isotherm of mpg-C_3N_4, XPS spectra of SnO_2/SnS_2/mpg-C_3N_4, optimization of experimental conditions, performance testing, photocurrents of different amount of feedstock of the as-synthesized materials, developed PEC immunosensors for detecting BNP compared with other published immunosensors, and the result of NT-proBNP determination in serum samples (PDF)

AUTHOR INFORMATION

Corresponding Authors

*E-mail: sdjndxwq@163.com. Phone: +86 531 82767872. Fax: +86 531 82767367 (Q.W.).

*E-mail: wangyaoguang9002@163.com. Phone: +86 531 82767872. Fax: +86 531 82767367 (Y.W.).

ORCID

Yong Zhang: 0000-0002-5831-637X

Qin Wei: 0000-0002-3034-8046

Yaoguang Wang: 0000-0003-0635-331X

Huangxian Ju: 0000-0002-6741-5302

Notes

The authors declare no competing financial interest.

DOI: 10.1021/acsami.8b11312
ACS Appl. Mater. Interfaces 2018, 10, 31080−31087

■ ACKNOWLEDGMENTS

This study was supported by the National Natural Science Foundation of China (nos. 21575050, 21627809, 21777056, 21775053), and Q.W. thanks the Special Foundation for Taishan Scholar Professorship of Shandong Province and UJN (no. ts20130937).

■ REFERENCES

(1) Toblli, J. E.; Lombraña, A.; Duarte, P.; Di Gennaro, F. Intravenous Iron Reduces NT-pro-Brain Natriuretic Peptide in Anemic Patients with Chronic Heart Failure and Renal Insufficiency. *J. Am. Coll. Cardiol.* **2007**, *50*, 1657−1665.

(2) Zelt, J. G. E.; Liu, P. P.; Erthal, F.; deKemp, R. A.; Wells, G.; O'Meara, E.; Garrard, L.; Beanlands, R. S. B.; Mielniczuk, L. M. NT-pro-Brain Natriuretic Peptide and HS-Troponin T Levels are Related to the Extent of Hibernating Myocardium in Patients with Ischemic Heart Failure. *Can. J. Cardiol.* **2017**, *33*, 1478−1488.

(3) Yanagisawa, D.; Ayusawa, M.; Kato, M.; Watanabe, H.; Komori, A.; Abe, Y.; Nakamura, T.; Kamiyama, H.; Takahashi, S. Factors Affecting N-Terminal Pro-Brain Natriuretic Peptide Elevation in the Acute Phase of Kawasaki Disease. *Pediatr. Int.* **2016**, *58*, 1105−1111.

(4) He, Y.; Wang, Y.; Yang, X.; Xie, S.; Yuan, R.; Chai, Y. Metal Organic Frameworks Combining $CoFe_2O_4$ Magnetic Nanoparticles as Highly Efficient Sers Sensing Platform for Ultrasensitive Detection of N-Terminal Pro-Brain Natriuretic Peptide. *ACS Appl. Mater. Interfaces* **2016**, *8*, 7683−7690.

(5) Li, H.; Yin, X.; Sun, D.; Xia, K.; Kang, C.; Chu, S.; Zhang, P.; Wang, H.; Qiu, Y. Detection of NT-pro BNP Using Fluorescent Protein Modified by Streptavidin as a Label in Immunochromatographic Assay. *Sens. Bio-Sens. Res.* **2016**, *11*, 1−7.

(6) Machen, M. C.; Oyama, M. A.; Gordon, S. G.; Rush, J. E.; Achen, S. E.; Stepien, R. L.; Fox, P. R.; Saunders, A. B.; Cunningham, S. M.; Lee, P. M.; Kellihan, H. B. Multi-Centered Investigation of a Point-of-Care NT-proBNP Elisa Assay to Detect Moderate to Severe Occult (Pre-Clinical) Feline Heart Disease in Cats Referred for Cardiac Evaluation. *J. Vet. Cardiol.* **2014**, *16*, 245−255.

(7) Shen, Q.; Han, L.; Fan, G.; Zhang, J.-R.; Jiang, L.; Zhu, J.-J. "Signal-on" Photoelectrochemical Biosensor for Sensitive Detection of Human T-Cell Lymphotropic Virus Type II DNA: Dual Signal Amplification Strategy Integrating Enzymatic Amplification with Terminal Deoxynucleotidyl Transferase-Mediated Extension. *Anal. Chem.* **2015**, *87*, 4949−4956.

(8) Toh, S. Y.; Citartan, M.; Gopinath, S. C. B.; Tang, T.-H. Aptamers as a Replacement for Antibodies in Enzyme-Linked Immunosorbent Assay. *Biosens. Bioelectron.* **2015**, *64*, 392−403.

(9) Wu, D.; Liu, Y.; Wang, Y.; Hu, L.; Ma, H.; Wang, G.; Wei, Q. Label-Free Electrochemiluminescent Immunosensor for Detection of Prostate Specific Antigen Based on Aminated Graphene Quantum Dots and Carboxyl Graphene Quantum Dots. *Sci. Rep.* **2016**, *6*, 20511.

(10) Han, Q.; Wang, R.; Xing, B.; Zhang, T.; Khan, M. S.; Wu, D.; Wei, Q. Label-Free Photoelectrochemical Immunoassay for CEA Detection Based on CdS Sensitized WO_3@BiOI Heterostructure Nanocomposite. *Biosens. Bioelectron.* **2018**, *99*, 493−499.

(11) Zhao, W.-W.; Xu, J.-J.; Chen, H.-Y. Photoelectrochemical Bioanalysis: The State of the Art. *Chem. Soc. Rev.* **2015**, *44*, 729−741.

(12) Fan, G.-C.; Zhu, H.; Du, D.; Zhang, J.-R.; Zhu, J.-J.; Lin, Y. Enhanced Photoelectrochemical Immunosensing Platform Based on CdSeTe@CdS:Mn Core-Shell Quantum Dots-Sensitized TiO_2 Amplified by CuS Nanocrystals Conjugated Signal Antibodies. *Anal. Chem.* **2016**, *88*, 3392−3399.

(13) Liu, Y.; Yan, K.; Zhang, J. Graphitic Carbon Nitride Sensitized with CdS Quantum Dots for Visible-light-driven Photoelectrochemical Aptasensing of Tetracycline. *ACS Appl. Mater. Interfaces* **2015**, *8*, 28255−28264.

(14) Liu, Y.; Li, R.; Gao, P.; Zhang, Y.; Ma, H.; Yang, J.; Du, B.; Wei, Q. A Signal-off Sandwich Photoelectrochemical Immunosensor Using TiO_2 Coupled with CdS as the Photoactive Matrix and Copper (II) Ion as Inhibitor. *Biosens. Bioelectron.* **2015**, *65*, 97−102.

(15) Fan, D.; Wu, D.; Cui, J.; Chen, Y.; Ma, H.; Liu, Y.; Wei, Q.; Du, B. An Ultrasensitive Label-free Immunosensor Based on CdS Sensitized Fe-TiO_2 with High Visible-light Photoelectrochemical Activity. *Biosens. Bioelectron.* **2015**, *74*, 843−848.

(16) Fan, G.-C.; Han, L.; Zhang, J.-R.; Zhu, J.-J. Enhanced Photoelectrochemical Strategy for Ultrasensitive DNA Detection Based on Two Different Sizes of CdTe Quantum Dots Cosensitized TiO_2/CdS:Mn Hybrid Structure. *Anal. Chem.* **2014**, *86*, 10877−10884.

(17) Liu, Y.; Zhang, Y.; Wu, D.; Fan, D.; Pang, X.; Zhang, Y.; Ma, H.; Sun, X.; Wei, Q. Visible-Light Driven Photoelectrochemical Immunosensor for Insulin Detection Based on MWCNTs@SnS_2@CdS Nanocomposites. *Biosens. Bioelectron.* **2016**, *86*, 301−307.

(18) Hu, L.; Chen, F.; Hu, P.; Zou, L.; Hu, X. Hydrothermal Synthesis of SnO_2/ZnS Nanocomposite as a Photocatalyst for Degradation of Rhodamine B under Simulated and Natural Sunlight. *J. Mol. Catal. A: Chem.* **2016**, *411*, 203−213.

(19) Raziq, F.; Qu, Y.; Humayun, M.; Zada, A.; Yu, H.; Jing, L. Synthesis of SnO 2 /B-P codoped g-C 3 N 4 nanocomposites as efficient cocatalyst-free visible-light photocatalysts for CO 2 conversion and pollutant degradation. *Appl. Catal., B* **2017**, *201*, 486−494.

(20) Wu, X.-F.; Zhang, C.-X.; Sun, Y.; Fu, S.-D.; Li, H.; Wang, Y.-J.; Zhang, J.-R.; Su, J.-Z.; Wang, Y.-W.; Wang, K.-Y. Preparation and Characterization of Nanosized Bi-Doped SnO_2/Reduced Graphene Oxide 3d Hybrids for Visible-light-driven Photocatalysis. *J. Nanosci. Nanotechnol.* **2018**, *18*, 4935−4939.

(21) Christoforidis, K. C.; Sengele, A.; Keller, V.; Keller, N. Single-Step Synthesis of SnS2 Nanosheet-Decorated TiO2 Anatase Nanofibers as Efficient Photocatalysts for the Degradation of Gas-Phase Diethylsulfide. *ACS Appl. Mater. Interfaces* **2015**, *7*, 19324−19334.

(22) Chen, H.; Gu, M.; Pu, X.; Zhu, J.; Cheng, L. Fabrication of SnO2@SnS2heterostructure with enhanced visible light photocatalytic activity. *Mater. Res. Express* **2016**, *3*, 065002.

(23) Su, F.; Mathew, S. C.; Lipner, G.; Fu, X.; Antonietti, M.; Blechert, S.; Wang, X. mpg-C3N4-Catalyzed Selective Oxidation of Alcohols Using O2and Visible Light. *J. Am. Chem. Soc.* **2010**, *132*, 16299−16301.

(24) Yang, Y.; Yang, X.-A.; Leng, D.; Wang, S.-B.; Zhang, W.-B. Fabrication of g-C_3N_4/SnS_2/SnO_2 Nanocomposites for Promoting Photocatalytic Reduction of Aqueous Cr(VI) under Visible Light. *Chem. Eng. J.* **2018**, *335*, 491−500.

(25) Fan, G.-C.; Zhu, H.; Du, D.; Zhang, J.-R.; Zhu, J.-J.; Lin, Y. Enhanced Photoelectrochemical Immunosensing Platform Based on CdSeTe@CdS:Mn Core−Shell Quantum Dots-Sensitized TiO_2 Amplified by CuS Nanocrystals Conjugated Signal Antibodies. *Anal. Chem.* **2016**, *88*, 3392−3399.

(26) Li, M.-J.; Zheng, Y.-N.; Liang, W.-B.; Yuan, R.; Chai, Y.-Q. Using P-Type PbS Quantum Dots to Quench Photocurrent of Fullerene-Au NP@MoS_2 Composite Structure for Ultrasensitive Photoelectrochemical Detection of ATP. *ACS Appl. Mater. Interfaces* **2017**, *9*, 42111−42120.

(27) Zhang, M.; Xu, J.; Zong, R.; Zhu, Y. Enhancement of visible light photocatalytic activities via porous structure of g-C3N4. *Appl. Catal., B* **2014**, *147*, 229−235.

(28) Wang, G.-L.; Liu, K.-L.; Shu, J.-X.; Gu, T.-T.; Wu, X.-M.; Dong, Y.-M.; Li, Z.-J. A Novel Photoelectrochemical Sensor Based on Photocathode of PbS Quantum Dots Utilizing Catalase Mimetics of Bio-Bar-Coded Platinum Nanoparticles/G-Quadruplex/Hemin for Signal Amplification. *Biosens. Bioelectron.* **2015**, *69*, 106−112.

(29) Liu, X.; Fu, F.; Xu, K.; Zou, R.; Yang, J.; Wang, Q.; Liu, Q.; Xiao, Z.; Hu, J. Folic Acid-Conjugated Hollow Mesoporous Silica/CuS Nanocomposites as a Difunctional Nanoplatform for Targeted Chemo-Photothermal Therapy of Cancer Cells. *J. Mater. Chem. B* **2014**, *2*, 5358−5367.

(30) Zhang, Y. C.; Yao, L.; Zhang, G.; Dionysiou, D. D.; Li, J.; Du, X. One-step hydrothermal synthesis of high-performance visible-light-

DOI: 10.1021/acsami.8b11312
ACS Appl. Mater. Interfaces 2018, 10, 31080−31087

driven SnS2/SnO2 nanoheterojunction photocatalyst for the reduction of aqueous Cr(VI). *Appl. Catal., B* **2014**, *144*, 730−738.
(31) Ye, L.; Liu, J.; Jiang, Z.; Peng, T.; Zan, L. Facets Coupling of BiOBr-g-C_3N_4 Composite Photocatalyst for Enhanced Visible-light-driven Photocatalytic Activity. *Appl. Catal., B* **2013**, *142−143*, 1−7.
(32) Wang, H.; Qi, C.; He, W.; Wang, M.; Jiang, W.; Yin, H.; Ai, S. A Sensitive Photoelectrochemical Immunoassay of N6-Methyladenosine Based on Dual-Signal Amplification Strategy: Ru Doped in SiO_2 Nanosphere and Carboxylated g-C_3N_4. *Biosens. Bioelectron.* **2018**, *99*, 281−288.
(33) Gao, P.; Ma, H.; Yan, T.; Wu, D.; Ren, X.; Yang, J.; Du, B.; Wei, Q. Construction of Dentate Bonded TiO_2-CdSe Heterostructures with Enhanced Photoelectrochemical Properties: Versatile Labels toward Photoelectrochemical and Electrochemical Sensing. *Dalton Trans.* **2015**, *44*, 773−781.
(34) Zhang, Y. C.; Du, Z. N.; Li, K. W.; Zhang, M.; Dionysiou, D. D. High-Performance Visible-light-driven SnS_2/SnO_2 Nanocomposite Photocatalyst Prepared Via in Situ Hydrothermal Oxidation of SnS_2 Nanoparticles. *ACS Appl. Mater. Interfaces* **2011**, *3*, 1528−1537.
(35) Wang, G.-L.; Xu, J.-J.; Chen, H.-Y.; Fu, S.-Z. Label-Free Photoelectrochemical Immunoassay for Alpha-Fetoprotein Detection Based on TiO_2/CdS Hybrid. *Biosens. Bioelectron.* **2009**, *25*, 791−796.
(36) Gao, E.; Wang, W.; Shang, M.; Xu, J. Synthesis and enhanced photocatalytic performance of graphene-Bi2WO6composite. *Phys. Chem. Chem. Phys.* **2011**, *13*, 2887−2893.

DOI: 10.1021/acsami.8b11312
ACS Appl. Mater. Interfaces 2018, 10, 31080−31087